

A far-red fluorescent protein evolved from a cyanobacterial phycobiliprotein

Erik A Rodriguez^{1,7}, Geraldine N Tran^{2,7}, Larry A Gross³, Jessica L Crisp¹, Xiaokun Shu^{4,5}, John Y Lin⁶ & Roger Y Tsien^{1,3}

Far-red fluorescent proteins (FPs) are desirable for *in vivo* imaging because with these molecules less light is scattered, absorbed, or re-emitted by endogenous biomolecules compared with cyan, green, yellow, and orange FPs. We developed a new class of FP from an allophycocyanin α -subunit (APC α). Native APC requires a lyase to incorporate phycocyanobilin. The evolved FP, which we named small ultra-red FP (smURFP), covalently attaches a biliverdin (BV) chromophore without a lyase, and has 642/670-nm excitation–emission peaks, a large extinction coefficient (180,000 M⁻¹cm⁻¹) and quantum yield (18%), and photostability comparable to that of eGFP. smURFP has significantly greater BV incorporation rate and protein stability than the bacteriophytochrome (BPH) FPs. Moreover, BV supply is limited by membrane permeability, and smURFPs (but not BPH FPs) can incorporate a more membrane-permeant BV analog, making smURFP fluorescence comparable to that of FPs from jellyfish or coral. A far-red and near-infrared fluorescent cell cycle indicator was created with smURFP and a BPH FP.

Fluorescent proteins (FPs) enable tracking of gene expression, cell fate, and fusion proteins^{1–4}. FPs from jellyfish or coral are spectrally limited to excitation maxima <610 nm, and they require oxygen for, and produce hydrogen peroxide upon, chromophore formation, thus requiring an aerobic environment tolerant of reactive oxygen species⁵. Chromophore formation may take hours⁵, and mixtures of green and red fluorescence are common^{6–8}. H₂O₂ is a mediator of cell survival, growth, differentiation, and implicated in diseases^{9–12}, which could complicate experimental results. Thus, FPs that use endogenous chromophores to eliminate oxygen necessity¹³ and hydrogen peroxide production are desirable. Far-red (FR) and near-infrared (NIR) FPs are desirable for imaging in living animals because these wavelengths minimize light scattering and absorbance by endogenous biomolecules and so reduce autofluorescence¹⁴. NIR FPs were engineered from non-fluorescent BPHs that attach biliverdin but have low quantum yield (QY) and protein stability^{15–20}.

We started with the light-harvesting phycobiliproteins from cyanobacteria (APC α from *Trichodesmium erythraeum*

(TeAPC α)). Native APC is a highly fluorescent hexamer (three α + β dimers) that uses an auxiliary protein known as a lyase to incorporate phycocyanobilin (PCB, Fig. 1a–c)²¹. Native APC biliprotein FPs have been created, but these FPs require a lyase, use PCB, and are expressed only in *Escherichia coli*^{22,23}. In our approach, we first evolved TeAPC α mutants to autocatalytically attach PCB (without a lyase) and fluoresce. Second, since PCB is not present in mammals, we evolved derivatives that bind BV (Fig. 1c), a molecule ubiquitous in eukaryotes and produced at the rate of 300–500 mg per d in humans²⁴. After 12 rounds of mutating and screening ~10⁶ bacterial colonies, an FP with 20 mutations was selected and named smURFP (homodimer-lacking chromophore, Fig. 1d).

RESULTS

Engineering and characterization of APC α FPs

We chose TeAPC α (15 kD) because it lacked 29 amino acids common to other APC α s (Supplementary Fig. 1). Expression of TeAPC α with heme oxygenase-1 (HO-1) and phycocyanobilin–ferredoxin oxidoreductase (PcyA) for PCB production showed no fluorescence (Fig. 2a). Round 1 (R1) of mutagenesis created an FP that covalently attached PCB (R1 + PCB) and was fluorescent (Supplementary Fig. 2a) with one mutation, N42I. Round 2 produced an FP (R2-1 + PCB) that was 27-fold brighter than R1 + PCB and had two mutations, Y65F and G66C, in the homodimeric interface. Round 3 produced R3-2 + PCB, with two mutations, V83I and V98M, and 1.7-fold brighter than R2-1 + PCB (Supplementary Fig. 2b). R2-1 + PCB and R3-2 + PCB had QYs of 7.2% and 13% and extinction coefficients (ECs) of 65,000 and 74,000 M⁻¹cm⁻¹, respectively, showing increased brightness (EC \times QY) correlated with biophysical properties.

After PCB selections, the PcyA gene was removed, leaving only BV production. R2-1 and R3-2 lacked fluorescence with BV. Round 4 produced an FP that covalently attached BV and had red-shifted fluorescence (R4-1; lack of PCB signifies BV). R4-1 contained four mutations, of which three (G45S, R61H, and Q129K) are necessary for BV covalent attachment. Round 5 selected R5-2 with two mutations, G4C and Y56H, which

¹Department of Pharmacology, University of California, San Diego, La Jolla, California, USA. ²School of Medicine, University of California, San Francisco, San Francisco, California, USA. ³Howard Hughes Medical Institute, La Jolla, California, USA. ⁴Department of Pharmaceutical Chemistry, University of California, San Francisco, San Francisco, California, USA. ⁵Cardiovascular Research Institute, University of California, San Francisco, San Francisco, California, USA. ⁶School of Medicine, University of Tasmania, Hobart, Tasmania, Australia. ⁷These authors contributed equally to this work. Correspondence should be addressed to E.A.R. (ear001@ucsd.edu) and R.Y.T. (rtsien@ucsd.edu).

Figure 2 | smURFP + BV-purified protein, spectra, and comparison of APC α and BPH FPs expressed in *E. coli* and smURFP + BV expressed *in vivo*. (a) Comparison of TeAPC α (expressed with PCB, but needs lyase for incorporation), smURFP + BV, and BV. Top is white light and bottom is fluorescence (EX/EM = 650/690 nm). (b) Normalized absorbance and fluorescence spectra of Cy5 and smURFP + BV. (c) Comparison of APC α and BPH FPs expressed in *E. coli*. *E. coli* was grown in LB + 0.02% arabinose at 37 °C for 17.5 h, and 2 ml of culture was resuspended in 1 ml PBS. Left and right are fluorescent images of FPs expressed in *E. coli* + HO-1, unless noted, and tubes are outlined in gray. Numbers in white are mean fluorescence intensity. Abs., absorbance; Fluor., fluorescence; EX, excitation maximum; EM, emission maximum; and LP, long pass.

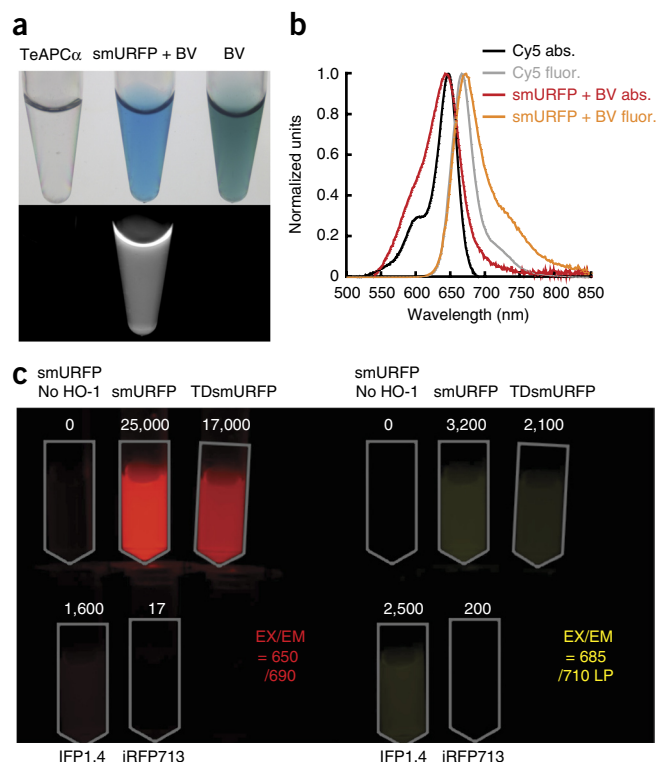
BV incorporation rate was measured in order to determine whether this was due to lack of BV and/or to smURFP's affinity for BV. smURFP fluorescence requires BV binding and covalent attachment. 0.5 μ M smURFP (1 μ M empty chromophore sites) was mixed with 0.1, 1, or 10 μ M BV (Supplementary Fig. 6). Fluorescence approached its asymptotic level as an exponential growth in time with a half-life \sim 39 min, independent of BV concentration, consistent with smURFP + BV forming a nonfluorescent high-affinity complex before development of fluorescence and covalent attachment to BV. Two-step kinetics are typical for phycobiliproteins and phytochromes^{26,27}. Increasing pH increases C52 nucleophilicity and the rate of fluorescence development (Supplementary Table 2). The low stoichiometry of BV relative to smURFP reflected limiting levels of BV during protein expression.

smURFP expression in neurons

smURFP fluorescence was compared to that of the coral-derived red FP mCherry, because fluorescence is spectrally separate from smURFP. Lentivirus was created with smURFP-T2A-mCherry, where T2A is a self-cleaving peptide sequence that ensures production of both FPs at a similar rate. Neuronal culture showed colocalized expression of both FPs. mCherry showed lysosomal aggregation²⁸, which is not seen with smURFP (Supplementary Fig. 7).

Increasing chromophore within mammalian cells

smURFP is better expressed than BPH FPs in bacteria (Fig. 2c). To test whether this was the case in mammalian cells, we expressed our constructs in HEK293A cells. smURFP and TDsmURFP



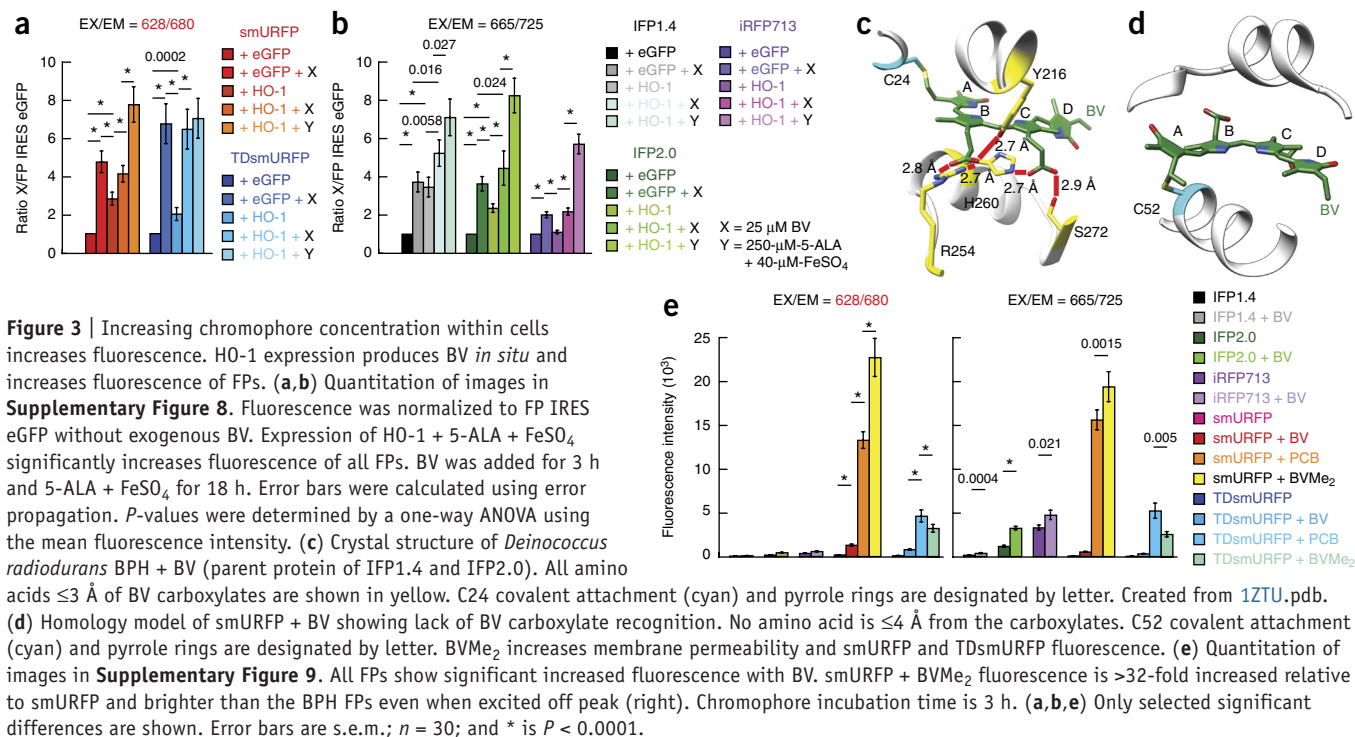
fluorescence is less than that of eGFP in HEK293A cells. We hypothesized that BV has low membrane permeability. 3 h of 25 μ M BV addition increased smURFP and TDsmURFP fluorescence by 4.7- and 6.7-fold, respectively (Fig. 3a). Purification of FP + BV in *E. coli* requires HO-1 to produce BV, and expression of HO-1 in mammalian cells should increase BV concentration. The production of heme is highly orchestrated (Supplementary Fig. 8a). Expression of cyanobacterial HO-1 with smURFP and TDsmURFP significantly increased fluorescence 2.8- and 2.0-fold, respectively. The expression of HO-1 with 5-aminolevulinic acid (5-ALA, a precursor of heme) and iron(ii) sulfate (to reduce the accumulation of fluorescent protoporphyrin IX (PpIX)) showed significant increases in smURFP and TDsmURFP fluorescence of 7.7- and 7.0-fold, respectively (Fig. 3a). To prove that the

Table 1 | Biophysical properties of FPs and Cy5

Fluorescent molecule	Excitation maximum (nm)	Emission maximum (nm)	Extinction coefficient ($M^{-1}cm^{-1}/$ chromophore)	Quantum yield (%)	<i>In vitro</i> photostability $t_{50\%}$ (s) ^a	Mammalian cell photostability $t_{50\%}$ (s) ^a	Stoichiometry	Chromophore maturation or attachment $t_{50\%}$ (min)	Protein stability $t_{50\%}$ (h) ^b	Molecular brightness relative to eGFP (%)
eGFP	488 ^c	507 ^c	56,000 ^c	60 ^c	110 ^c	560	Monomer	25 ^c	21	100
mCherry	587 ^c	610 ^c	72,000 ^c	22 ^c	96 ^c	89	Monomer	15 ^c		47
mCardinal	604 ^d	659 ^d	87,000 ^d	19 ^d	730 ^d		Monomer	27 ^d		49
smURFP + BV	642	670	180,000	18	300	570	Dimer	39	33	96
smURFP + BVMe ₂	646	672	65,000	12		340	Dimer		35	23
TDsmURFP + BV	642	670	170,000	18	190		Tandem dimer			91
iRFP670	643 ^e	670 ^e	114,000 ^e	11 ^e		290 ^e	Dimer			37
Cy5	649	670	250,000	25	22		NA		NA	186
IFP1.4	684 ^f	708 ^f	92,000 ^f	7 ^f	8.4 ^f	70 ^e , 50 ^g	Weak dimer	114 ^g	4.4 ^g	19
IFP2.0	690 ^h	711 ^h	86,000 ^h	8 ^h			Weak dimer			20
iRFP713	690 ^g	713 ^g	98,000 ^g	6.3 ^e , 5.9 ^g		960 ^e , 450 ^g	Dimer	168 ^g	\sim 4.4 ^g	18

Photostability, time to bleach 50% from an initial emission rate of 1,000 photons per s. NA, not applicable. ^aDetermined as described in ref. 3. ^bDetermined as described in Online Methods.

^cData from ref. 3. ^dData from ref. 29. ^eData from ref. 17. ^fData from ref. 15. ^gData from ref. 16. ^hData from ref. 18.



benefit of extra BV is not limited to smURFP, we expressed HO-1 with BPH FPs. IFP1.4, IFP2.0, and iRFP713 all showed significant increases in fluorescence of 7.1-, 8.2-, and 5.7-fold, respectively, with HO-1 + 5-ALA + FeSO₄, even though it was reported that iRFP713 does not require exogenous BV¹⁶ (Fig. 3b).

The more hydrophobic biliverdin dimethylester (BVMe₂, Fig. 1c) should have greater membrane permeability. The carboxylic acids of BV are recognition motifs and must be free for BPHs, while carboxylic groups of BV are exposed on smURFP and tolerate esterification (Fig. 3c,d). Addition of 25 μ M BV for 3 h significantly increased fluorescence of BPH FPs (Fig. 3e and Supplementary Fig. 9). Addition of 25 μ M BVMe₂ or PCB (for 3 h in each case) greatly increased smURFP fluorescence—by 18- and 10-fold, respectively—relative to 25 μ M BV (Fig. 3e). TDsmURFP was brightened by 4.0- and 5.8-fold with BVMe₂ and PCB, respectively. 25 μ M PCB added to IFP2.0 blue shifted and decreased fluorescence. IFP2.0 + 25 μ M BVMe₂ resulted in no fluorescence increase (Supplementary Fig. 10), indicating that esterases do not remove methyl groups on BVMe₂ to form BV, which would enhance the fluorescence of IFP2.0. smURFP + BVMe₂ is ≥ 7 -fold brighter than IFP2.0 or iRFP713 (Fig. 3e).

The concentration dependence of different chromophores was also analyzed (Supplementary Fig. 11). PCB requires ≥ 40 μ M for fluorescence similar to 2.5 μ M BVMe₂. BVMe₂ penetrates the membrane best, reaching saturation at ≤ 2.5 μ M. We expressed eGFP from an internal ribosomal entry site (IRES) along with smURFP expressed from the CMV promoter in the presence of BVMe₂. Under these conditions, eGFP expression was lower relative to smURFP, and smURFP had five-fold greater fluorescence. Based on photophysical properties, smURFP is as bright as eGFP and could be equally bright in mammalian cells with sufficient chromophore in the cytoplasm.

BV contains two anionic carboxylates. Acidification protonates the carboxylates and increases BV permeability. 25 μ M BV added

at pH 6.4 for 3.5 h increased fluorescence three-fold relative to BV at pH 7.5. As controls, BVMe₂ incorporation or eGFP expression were not affected by a drop in extracellular pH from 7.5 to 6.4 over 3.5 h, showing no change in protein stability, protein translation, and cell health. Protonation of BV increased membrane permeability, but fluorescence was five-fold less than that of BVMe₂.

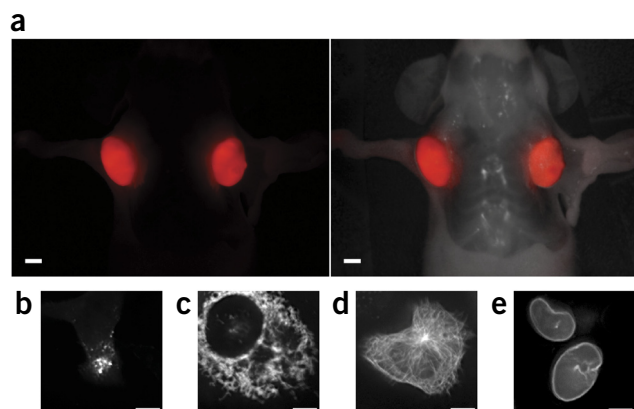
smURFP and TDsmURFP with different chromophores

smURFP and TDsmURFP have two chromophore sites, but the predominant species contains only 1 BV. smURFP and TDsmURFP were expressed without HO-1 and purified without chromophore, then chromophores were added *in vitro*. Samples were verified with MS (Supplementary Fig. 12), and biophysical properties were measured. For BV and PCB, two chromophores could attach, but the second chromophore partially quenched fluorescence and reduced the QY (Supplementary Table 3). Two PCBs had a 40-nm red-shifted fluorescence (Supplementary Fig. 13g,i). A single BVMe₂ bound to smURFP, while two BVMe₂ bound to TDsmURFP (Supplementary Fig. 12f,i). For BVMe₂, the QY of 12% remained constant. smURFP or TDsmURFP + BVMe₂ have the brightest fluorescence, not only because BVMe₂ is freely membrane permeant, but because the fluorescence is not quenched by excess chromophore.

smURFP *in vivo*

In order to test smURFP performance *in vivo*, HT1080 cells were transduced with lentivirus ($\geq 99\%$ efficiency) to express smURFP and mCherry (Supplementary Fig. 14a). smURFP and mCherry fluorescence in the HT1080 cells *in vitro* were equivalent when the cells were incubated in 12.5 μ M BV for 3 h (Supplementary Fig. 14b). HT1080 cells stably expressing smURFP and mCherry were injected into four mice bearing two tumor xenografts. smURFP fluorescence was visible without exogenous BV (Fig. 4a), but fluorescence intensity was 35% of that of mCherry

Figure 4 | smURFP expressed *in vivo* and smURFP fusions in mammalian cells. (a) Representative image of smURFP expressed in two HT1080 tumor xenografts without exogenous BV. Fluorescence only (left) and overlay of fluorescence and mouse body (right). Data from three additional mice are shown in **Supplementary Figure 14**. Scale bars, 0.5 cm. (b–d) PC3 cells were transfected with DNA, and FP fusions were imaged 48 h later after incubation with 25 μ M BV for 4 h. Fusions at the smURFP N terminus: (b) ManII-10aa-smURFP + BV (mouse, mannosidase II, and Golgi complex) and (c) PDHA1-10aa-smURFP + BV (human, pyruvate dehydrogenase, and mitochondria). Fusions at the smURFP C terminus: (d) smURFP + BV-18aa- α Tub (human, α -tubulin, and microtubules) and (e) smURFP + BV-10aa-LamB1 (human, lamin B1, and nuclear envelope). (b–e) Cell images are representative of >20 imaged cells. Similar images were obtained with incubation of 1 μ M BVMe₂. Scale bars, 10 μ m. No. aa, linker length in amino acids and in parentheses: (protein origin, protein name, and cellular location).

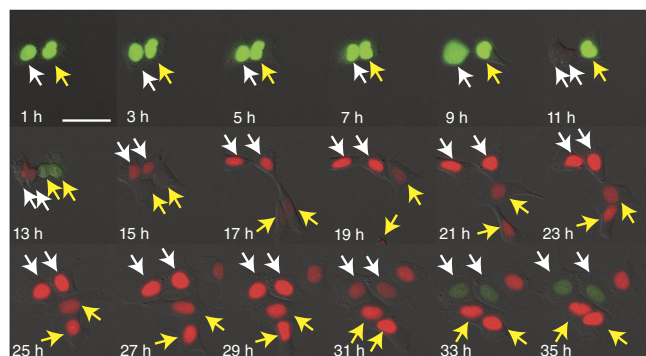


(**Supplementary Fig. 14c,d**). 250 nmol BV was injected intravenously, but no fluorescence increase was seen after 2 h. Fluorescence of mCherry was greatly attenuated through the skin with a loss of 74%, while smURFP had a loss of only 25%, illustrating the importance of using FR and NIR FPs for deep-tissue imaging (**Supplementary Fig. 14e**).

smURFP was compared to mCardinal²⁹ in smaller tumors in an area with less blood flow (**Supplementary Fig. 15**). HT1080 cells were transduced with lentivirus expressing smURFP or mCardinal ($\geq 95\%$ efficiency) (**Supplementary Fig. 15a**). The FPs were separated because of significant spectral overlap. smURFP is 2- to 4-fold brighter than mCardinal when BVMe₂ is added for 2 d (**Supplementary Fig. 15c–e**), but smURFP is much dimmer than mCardinal *in vivo* (~ 7.3 -fold at 607 nm and ~ 4 -fold at 640 nm, **Supplementary Fig. 15f**). Injection of 250 nmol BV or BVMe₂ gives no increase in fluorescence *in vivo*, though 10 μ M BV or BVMe₂ added to excised tumors enhanced fluorescence and verified smURFP expression (**Supplementary Fig. 15g**). 10 μ M BV or BVMe₂ added to plasma showed rapid removal of ester groups and slower degradation of impermeant BV (**Supplementary Fig. 16**), which explained the discrepancy.

FP stability

FP stability influences expression and fluorescence intensity. eGFP has a protein stability half-life ($t_{50\%}$) of ~ 24 h³⁰, while BPH FPs have $t_{50\%}$ of ~ 4.4 h (**Table 1**). The fluorescence of smURFP in HEK293 cells continuously exposed to BV or BVMe₂, but with protein synthesis halted by cycloheximide, declined with $t_{50\%} = 33$ or 35 h, respectively (**Supplementary Fig. 17a,b**). Shortening exposure of BV or BVMe₂ to 3 h produced little difference ($t_{50\%} = 30$ h and 33 h, respectively) (**Supplementary Fig. 17c,d**).



The lifetime of smURFP lacking chromophore was determined by addition of cycloheximide for various time periods, and BVMe₂ was added for 1 h. Apoprotein decayed with $t_{50\%} = 17$ h (**Supplementary Fig. 17e**), showing a modest destabilization. As a control, eGFP had a $t_{50\%} = 21$ h, close to 24 h³⁰ (**Supplementary Fig. 17f**). smURFP initial mean fluorescence shows that membrane permeability is the major factor increasing fluorescence under nonsteady state conditions, but increasing incubation time results in increased protein stability and accumulation of smURFP + chromophore (**Supplementary Fig. 17g**).

FP photostability and performance in fusions

smURFP and TDsmURFP show greater photostability than eGFP, mCherry, IFP1.4, and Cy5 *in vitro* (**Supplementary Fig. 18**). The protein, rather than the BV, governs the photostability, because at an excitation intensity yielding 1,000 photons per s, IFP1.4 + BV bleached with $t_{50\%} = 8.4$ s, while smURFP + BV had $t_{50\%} = 300$ s (**Table 1**). Photostability was compared in cells. N- and C-terminal smURFP fusions were created and showed correct cellular localization (**Fig. 4**). smURFP mean $t_{50\%}$ was 340 s and 570 s with BVMe₂ and BV, respectively, in mammalian cells (**Supplementary Fig. 19**). smURFP + BV photostability is comparable to that of eGFP but greater than that of mCherry and tdTomato (**Supplementary Table 4**).

An FR and NIR fluorescent cell cycle biosensor

Based on work from Miyawaki and coworkers⁴ on the fluorescent ubiquitination-based cell cycle indicator (FUCCI), we created a fluorescent biosensor at wavelengths longer than attainable with jellyfish- or coral-derived FPs using smURFP and IFP2.0 (ref. 18). In FUCCI, two spectrally distinct FPs are synthesized and degraded at opposing phases of the cell cycle. Typically a green FP is made during S, G₂, or M phase and degraded during late M or G₁ phase, while an orange FP is made during G₀ or G₁ phase and destroyed at the start of S phase⁴. smURFP, TDsmURFP, and IFP2.0 were fused to hCdt1(30/120) and hGem(1/110) fragments containing ubiquitination sites for degradation⁴. Stable HEK293A cell

Figure 5 | Time-lapse microscopy of FR and NIR FUCCI expressed in HEK293A cells. IFP2.0-hGem(1/110) and smURFP-hCdt1(30/120) fluorescence are shown in green and red, respectively. White and yellow arrows label original cells and their descendants. HEK293A cell division occurs with a doubling time of ~ 34 h. Green is EX/EM = 665(45)/725(50) nm, and red is EX/EX = 628(40)/680(30) nm. Scale bar, 50 μ m.

lines were created. smURFP fluorescence was greater than that of TDsmURFP. A stable cell line expressing mAG-hGem(1/110) and smURFP-hCdt1(30/120) was created to verify proper function. smURFP-hCdt1(30/120) showed proper temporal dynamics (Supplementary Fig. 20 and Supplementary Video 1). Stably expressing IFP2.0-hGem(1/110) showed sufficient fluorescence, but IFP2.0-hCdt1(30/120) did not. Fluorescence time-lapse imaging verified that HEK293 cells stably expressing smURFP-hCdt1(30/120) and IFP2.0-hGem(1/110) reciprocally lit up during the G₀ or G₁ and S, G₂, or M phases, respectively (Fig. 5 and Supplementary Video 2). FUCCI now works in the FR and NIR.

DISCUSSION

smURFP is biophysically the brightest FR and NIR FP created, fills a spectral gap in excitation wavelength, expresses efficiently with minimal toxicity, and does not produce hydrogen peroxide. In addition, unlike its precursor, TeAPC α , smURFP does not require a lyase to covalently attach its chromophore.

smURFP fluorescence is visible without exogenous BV and may be advantageous for imaging cancer or other maladies *in vivo*, where the production of hydrogen peroxide could alter immune system or inflammation response and/or alter disease progression^{9–12}. Here, it is important to note that previous comparisons of BPH FPs and red FPs *in vivo* were performed using purified FPs, normalizing concentrations with BV already covalently attached, and by embedding FPs inside phantoms into mice^{16,17}. This experimental setup does not accurately reflect FP expression and accessibility to BV *in vivo* where, for example, iRFP713 shows little fluorescence when compared to mCardinal²⁹.

Membrane permeability of BV is a limiting factor for BPH FPs and smURFP. The development of smURFP fluorescence is controlled by the covalent attachment of the cofactor, not by reversible noncovalent BV affinity. HO-1 expression in neurons increases IFP2.0 fluorescence¹⁸. HO-1 increased fluorescence significantly for BPH and APC α FPs, and it enhanced more with 5-ALA and iron, which fuel production of heme that HO-1 converts to BV. smURFP and TDsmURFP, unlike BPH FPs, tolerate the freely permeant BVMe₂. This open chromophore-binding pocket (Fig. 3d) should allow for further modification of tetrapyrroles to modify not only membrane permeability but also spectral and fluorescence properties.

FP photostability is essential for imaging extended time periods or super-resolution. BPH FPs were originally nonfluorescent phototransducers that lacked evolutionary pressure to be light tolerant, whereas APC α is a component of the light-harvesting phycobilisome, which is extremely tolerant of light. Without using a special selection, smURFP is very photostable. Selection for increased photostability should enhance smURFP utility for super-resolution applications.

The FR and NIR FUCCI creates a fluorescent biosensor with wavelengths inaccessible to jellyfish or coral FPs and does not produce hydrogen peroxide. Fluorescently monitoring the cell cycle has identified modifications to cell division, drug-induced cell cycle modification³¹, and quiescent cells³².

smURFP is brighter than mCardinal *in vitro* when BVMe₂ is added for 2 d, and it is comparable to eGFP in brightness, which is useful in cell culture for imaging low-copy-number proteins, super-resolution imaging, and biosensors (FRET acceptor or red FP quencher). Despite its strong performance *in vitro* and modest

visibility *in vivo*, smURFP is not ready for use in mice, as this will require screening new cofactors to achieve maximal brightness. smURFP is the most photostable FP tested in the Tsien lab (all FPs tested by P. Steinbach for over 10 years³). smURFP can be fused to α -tubulin (Fig. 4d), one of the most sensitive proteins. In addition, smURFP is one of only three FPs (smURFP, mKO2, and mCherry) known to allow functional fusion to hCdt1(30/120) despite the fact that jellyfish- or coral-derived FPs mAG, eGFP, and mRFP1 are nonfunctional⁴. The FR and NIR FUCCI is the first biosensor using two BV-attaching FPs and can be used with traditional FUCCI to monitor the cell cycle of two cell types.

There are thousands of APC α genes in cyanobacteria and red algae, giving this new class of FPs vast opportunities. Additionally, APC β and other phycobilisome proteins (phycoerythrin and phycocyanin) could be used to create additional FPs.

METHODS

Methods and any associated references are available in the [online version of the paper](#).

Accession codes. GenBank/EMBL/DDBJ: smURFP, KX449134; TDsmURFP, KX449135. Bacterial and mammalian expression plasmids and lentiviral transfer vectors are available at Addgene: smURFP, 80341, 80343, 80345, 80347, 80348, 80349; TDsmURFP, 80342, 80344, 80346.

Note: Any Supplementary Information and Source Data files are available in the online version of the paper.

ACKNOWLEDGMENTS

National Institute of General Medical Sciences Postdoctoral Fellowship F32GM089114 supported the project (E.A.R.). US National Institutes of Health grants GM086197 (R.Y.T.), NS027177 (R.Y.T.), NS090590 (J.Y.L.), and the Howard Hughes Medical Institute (R.Y.T.) supported the project. We thank P. Steinbach for measuring photostability, Q. Xiong for FACS, S. Adams for advice and experimental expertise, and P. Arcaira for help with mouse experiments. We thank M. Lin (Departments of Pediatrics and Bioengineering, Stanford, Stanford, CA) for iRFP713 vectors, M. Davidson (Addgene) for fusion vectors, and A. Miyawaki (Laboratory for Cell Function Dynamics, RIKEN Brain Science Institute, Wako, Japan) for FUCCI vectors. This paper is dedicated to the memory of Roger Tsien, who passed away shortly after it was published.

AUTHOR CONTRIBUTIONS

E.A.R. and G.N.T. created bacterial expression plasmids, evolved and developed smURFP and APC α FPs in *E. coli*, and characterized properties. E.A.R. prepared mammalian plasmids, made the smURFP homology model, created TDsmURFP, performed BV incorporation rates, performed mammalian cell experiments (HO-1, different chromophores, protein stability, and FP photobleaching), created FR and NIR FUCCI, and performed fluorescence imaging *in vitro* and *in vivo*. J.Y.L. transduced neurons. E.A.R. and J.Y.L. created virus and stable HT1080 cells for mouse models. J.Y.L. and J.L.C. injected animals with cancer cells and chromophores. J.L.C. prepared plasma. E.A.R., G.N.T., and J.Y.L. purified PCB and analyzed data. L.A.G. performed MS. X.S. chose the *Trichodesmium* APC α gene and oversaw the first three rounds of evolution of APC α + PCB. R.Y.T. and E.A.R. oversaw the design and analysis of the experiments. All authors contributed to writing and discussion.

COMPETING FINANCIAL INTERESTS

The authors declare no competing financial interests.

Reprints and permissions information is available online at <http://www.nature.com/reprints/index.html>.

1. Giepmans, B.N., Adams, S.R., Ellisman, M.H. & Tsien, R.Y. The fluorescent toolbox for assessing protein location and function. *Science* **312**, 217–224 (2006).
2. Tsien, R.Y. Constructing and exploiting the fluorescent protein paintbox (Nobel lecture). *Angew. Chem. Int. Edn. Engl.* **48**, 5612–5626 (2009).

3. Shaner, N.C., Steinbach, P.A. & Tsien, R.Y. A guide to choosing fluorescent proteins. *Nat. Methods* **2**, 905–909 (2005).
4. Sakaue-Sawano, A. *et al.* Visualizing spatiotemporal dynamics of multicellular cell-cycle progression. *Cell* **132**, 487–498 (2008).
5. Tsien, R.Y. The green fluorescent protein. *Annu. Rev. Biochem.* **67**, 509–544 (1998).
6. Shaner, N.C. *et al.* Improved monomeric red, orange and yellow fluorescent proteins derived from *Discosoma sp.* red fluorescent protein. *Nat. Biotechnol.* **22**, 1567–1572 (2004).
7. Moore, M.M., Oteng-Pabi, S.K., Pandelieva, A.T., Mayo, S.L. & Chica, R.A. Recovery of red fluorescent protein chromophore maturation deficiency through rational design. *PLoS ONE* **7**, e52463 (2012).
8. Tubbs, J.L., Tainer, J.A. & Getzoff, E.D. Crystallographic structures of *Discosoma* red fluorescent protein with immature and mature chromophores: linking peptide bond *trans-cis* isomerization and acylimine formation in chromophore maturation. *Biochemistry* **44**, 9833–9840 (2005).
9. Veal, E.A., Day, A.M. & Morgan, B.A. Hydrogen peroxide sensing and signaling. *Mol. Cell* **26**, 1–14 (2007).
10. Hussain, S.P., Hofseth, L.J. & Harris, C.C. Radical causes of cancer. *Nat. Rev. Cancer* **3**, 276–285 (2003).
11. Weitzman, S.A. & Gordon, L.I. Inflammation and cancer: role of phagocyte-generated oxidants in carcinogenesis. *Blood* **76**, 655–663 (1990).
12. Barnham, K.J., Masters, C.L. & Bush, A.I. Neurodegenerative diseases and oxidative stress. *Nat. Rev. Drug Discov.* **3**, 205–214 (2004).
13. Kumagai, A. *et al.* A bilirubin-inducible fluorescent protein from eel muscle. *Cell* **153**, 1602–1611 (2013).
14. König, K. Multiphoton microscopy in life sciences. *J. Microsc.* **200**, 83–104 (2000).
15. Shu, X. *et al.* Mammalian expression of infrared fluorescent proteins engineered from a bacterial phytochrome. *Science* **324**, 804–807 (2009).
16. Filonov, G.S. *et al.* Bright and stable near-infrared fluorescent protein for *in vivo* imaging. *Nat. Biotechnol.* **29**, 757–761 (2011).
17. Shcherbakova, D.M. & Verkhusha, V.V. Near-infrared fluorescent proteins for multicolor *in vivo* imaging. *Nat. Methods* **10**, 751–754 (2013).
18. Yu, D. *et al.* An improved monomeric infrared fluorescent protein for neuronal and tumour brain imaging. *Nat. Commun.* **5**, 3626 (2014).
19. Auldridge, M.E., Satyshur, K.A., Anstrom, D.M. & Forest, K.T. Structure-guided engineering enhances a phytochrome-based infrared fluorescent protein. *J. Biol. Chem.* **287**, 7000–7009 (2012).
20. Fischer, A.J. & Lagarias, J.C. Harnessing phytochrome's glowing potential. *Proc. Natl. Acad. Sci. USA* **101**, 17334–17339 (2004).
21. Yeh, S.W., Ong, L.J., Clark, J.H. & Glazer, A.N. Fluorescence properties of allophycocyanin and a crosslinked allophycocyanin trimer. *Cytometry* **8**, 91–95 (1987).
22. Tooley, A.J., Cai, Y.A. & Glazer, A.N. Biosynthesis of a fluorescent cyanobacterial C-phycoerythrin holo- α subunit in a heterologous host. *Proc. Natl. Acad. Sci. USA* **98**, 10560–10565 (2001).
23. Zhang, J. *et al.* Fused-gene approach to photoswitchable and fluorescent biliproteins. *Angew. Chem. Int. Edn. Engl.* **49**, 5456–5458 (2010).
24. Harris, J.W. & Kellermeyer, R.W. *The Red Cell: Production, Metabolism, Destruction: Normal and Abnormal*, Revised edn. (Harvard University Press, 1970).
25. Wahleithner, J.A., Li, L.M. & Lagarias, J.C. Expression and assembly of spectrally active recombinant holophytochrome. *Proc. Natl. Acad. Sci. USA* **88**, 10387–10391 (1991).
26. Arciero, D.M., Bryant, D.A. & Glazer, A.N. *In vitro* attachment of bilins to apophycocyanin. I. Specific covalent adduct formation at cysteinyl residues involved in phycocyanobilin binding in C-phycoerythrin. *J. Biol. Chem.* **263**, 18343–18349 (1988).
27. Li, L., Murphy, J.T. & Lagarias, J.C. Continuous fluorescence assay of phytochrome assembly *in vitro*. *Biochemistry* **34**, 7923–7930 (1995).
28. Katayama, H., Yamamoto, A., Mizushima, N., Yoshimori, T. & Miyawaki, A. GFP-like proteins stably accumulate in lysosomes. *Cell Struct. Funct.* **33**, 1–12 (2008).
29. Chu, J. *et al.* Noninvasive intravital imaging of cellular differentiation with a bright red-excitable fluorescent protein. *Nat. Methods* **11**, 572–578 (2014).
30. Stack, J.H., Whitney, M., Rodems, S.M. & Pollok, B.A. A ubiquitin-based tagging system for controlled modulation of protein stability. *Nat. Biotechnol.* **18**, 1298–1302 (2000).
31. Sakaue-Sawano, A., Kobayashi, T., Ohtawa, K. & Miyawaki, A. Drug-induced cell cycle modulation leading to cell-cycle arrest, nuclear mis-segregation, or endoreplication. *BMC Cell Biol.* **12**, 2 (2011).
32. Tomura, M. *et al.* Contrasting quiescent G0 phase with mitotic cell cycling in the mouse immune system. *PLoS ONE* **8**, e73801 (2013).

ONLINE METHODS

Chemicals. BV and BVMe₂ were purchased from Frontier Scientific. PCB was extracted from *Spirulina* as described³³.

Gene synthesis, mutagenesis, and screening of libraries. TeAPC α gene (codons optimized for *Escherichia coli*) was made by GenScript. Mutations were placed by random mutagenesis using GeneMorphII Random Mutagenesis Kit (Agilent Technologies). Screens for mutants that fluoresce with PCB or BV were performed by subcloning into a pBAD vector (Life Technologies) that expressed cyanobacteria *Synechocystis* HO-1 and *Synechocystis* PcyA genes for PCB production and *Synechocystis* HO-1 only for BV production, as previously described³⁴. Libraries were expressed in TOP10 Electrocompetent *Escherichia coli* cells (Life Technologies) with addition of 0.2% arabinose to LB agar plates (FPs were constitutively expressed in *Escherichia coli*). Fluorescence was imaged on plates using a BioSpectrum AC Imaging System (UVP) with EX/EM = 628(40)/690(50) nm for FPs + PCB, EX/EM = 685(40)/710LP nm for rounds 4 and 5 FPs + BV, and EX/EM = 650(13)/690(50) nm for Cy5-like FPs + BV (rounds 6–12). At round 6, 5–10 of the brightest colonies on each plate were combined in LB + 0.2% arabinose, grown ~18 h, mixture of plasmid DNA was purified, and TOP10 cells were transformed and plated on LB agar plates + 0.2% arabinose. Fluorescence was screened on plates (as described above), 10–20 of the brightest colonies were screened in liquid culture fluorescence (Supplementary Fig. 2a–e), plasmid DNA was purified, and DNA was sequenced. The plasmid DNA of 2–3 of the brightest FPs was chosen for mutagenesis for the subsequent round. When choosing DNA for subsequent mutagenesis rounds, genes with increased and/or novel silent DNA mutations were chosen over other DNA that had the same DNA and/or protein sequence of the previous round. Site-specific mutagenesis was performed using QuikChange Lightning Mutagenesis Kit (Agilent Technologies) to create smURFP (C4S mutation) and smURFP C52S.

FP purification and fluorescence characterization *in vitro*. FP genes were expressed on a pBAD vector (Life Technologies) with a polyhistidine tag on the C terminus, cells were lysed with B-PER (Thermo Scientific), and purified using Ni-NTA (Qiagen) purification. PCB (HO-1 + PcyA) and BV (HO-1) incorporation in *Escherichia coli* was performed simultaneously during constitutively active FP expression. Extinction coefficient was determined by PCB or BV absorbance as described^{35,36} (Table 1, smURFP + BV and TDsmURFP + BV, and Supplementary Table 1) or calculated for the apoproteins by determining the protein concentration by the BCA protein assay (Pierce), and a specific chromophore concentration was added (specified in the Purification of FP lacking chromophore and *in vitro* chromophore incorporation section) to get 1 and 2 chromophore species (Supplementary Table 3, not including (*Escherichia coli*)). When FP chromophore (PCB or BV) was expressed in *Escherichia coli*, the PCB and BV Q band had absorbance that overlapped with detection of BCA or Bradford assay of 562 nm and 592 nm, respectively. We used the previously published protocols^{35,36}, where there was no change of the BV absorbance at 390 nm when free in solution or attached to the FP. smURFP + BV denaturation with 1 M urea caused no change in the BV absorbance at 390 nm, but the Q band was reduced ~20-fold. Therefore, the extinction coefficient of BV at

390 nm was used to calculate the concentration of holoprotein (FP + PCB or BV) concentration.

EX and EM spectra were obtained using SPEX Fluorolog fluorometer (Horiba). Absorbance spectra were obtained using UV-VIS Spectrophotometer Cary Eclipse (Varian) or UV-2700 (Shimadzu). Quantum yield was determined relative to Cy5. Incorporation rates of BV on 0.5 μ M smURFP was performed by addition of smURFP to PBS alone or with 20% fetal bovine serum (FBS) and mixed by pipetting in a quartz cuvette. Chromophore was added last, mixed by pipetting, and fluorescence was recorded using SPEX Fluorolog fluorometer (Horiba). Photobleaching was characterized on bubbles of purified FP or Cy5 within mineral oil using light from a 150 W xenon arc lamp with 100% light through EX/EM = 628(40)/680(30) nm for smURFP, TDsmURFP, and Cy5 or EX/EM = 665(45)/725(50) nm for IFP1.4 focused with a 40 \times , 1.2 numerical aperture C-Apochromat oil-immersion lens on a Zeiss Axiovert 200M inverted microscope. Photobleaching times were normalized to reflect an initial illumination intensity producing 1,000 photons per fluorescent molecule per second as previously described³⁷.

Purification of FP lacking chromophore and *in vitro* chromophore incorporation. HO-1 was removed by digesting the pBAD vector (Life Technology) with MscI and PmeI (NEB). smURFP and TDsmURFP were expressed and purified as described above. No chromophore was present on smURFP and TDsmURFP (confirmed by UV, fluorescence imaging, and MS). For predominant fluorescent species + 2 chromophores, a ten-fold excess of chromophore was added to smURFP and TDsmURFP. For predominant fluorescent species + 1 chromophore, a quarter concentration of chromophore was added to smURFP and TDsmURFP. Chromophore was added in PBS + 10% FBS at 37 °C overnight. smURFP + chromophore and TDsmURFP + chromophore were purified using NiNTA (Qiagen) to remove excess or noncovalently attached chromophore.

FP mass spectrometry. FP mass was determined by liquid chromatography–mass spectrometry (LC–MS), where the protein column eluant was directly injected into the electrospray interface of an Orbitrap XL (Thermo Fisher). FP precipitation was minimized by using a steep gradient and injecting column eluant directly into the mass spectrometer. The 1100 LC (Agilent Technologies) had solvent A = 2% acetonitrile (ACN), 0.1% formic acid (FA) and solvent B = 90% ACN, 0.1% FA, the flow rate was 80 μ L/min, and the gradient was 18% A to 100% B in 2.4 min. Protein was eluted within 10 min from a 1 mm inner diameter, 50 mm long PLRP-S C18 column (Agilent Technologies). Orbitrap IonSpray (electrospray) interface had a sheath gas flow rate of 34 and T = 275 °C. Capillary was 39 V and the tube lens was 140 V. Full scan mass spectra were collected in the ion trap and Fourier transform profile mode, with Orbitrap resolution 60,000, from 500 to 1,800 mass-to-charge units. Protein mass spectra were deconvolved using either the extract_msn program (Xcalibur software) or with ProMassCalc (ThermoFisher).

Homology model creation, identifying dimeric interface, protein sequence alignment, and creating protein figures. smURFP homology model was created using Swiss-Model Server³⁸ with *Porphyrizyezoensis* APC α crystal structure (1KN1.pdb³⁹

(<http://www.rcsb.org/pdb/explore.do?structureId=1KN1>) and sequence in **Supplementary Fig. 1**). The homodimeric interface was identified using PatchDock⁴⁰ and, subsequently, FireDock⁴¹. The lowest free-energy structure is shown in **Figure 1d**. Protein sequence alignments (**Supplementary Figs. 1 and 2**) were created using ClustalX⁴². All protein figures were created using UCSF Chimera package⁴³.

Construction of TDsmURFP bacterial expression vector. TDsmURFP was created using the smURFP homology model (**Fig. 1d**) and approximating the distance from the C terminus to the N terminus of the second subunit. A 23-amino-acid linker (GHGTGSTGSGSGTASSEDNNMA) was sufficient, and primers were created with 5' BamHI and 3' EcoRI restriction sites (Integrated DNA Technologies, IDT) smURFP was PCR amplified with Phusion High-Fidelity DNA Polymerase (New England BioLabs, NEB) to create the right and left subunits using 23-amino-acid linker primers. The two products were combined, and TDsmURFP was created by bridging PCR with Phusion High-Fidelity DNA Polymerase (NEB). TDsmURFP was digested with BamHI-HF and EcoRI-HF (NEB), gel purified using Zymoclean Gel DNA Recovery Kit (Zymo), and subcloned into a pBAD (Life Technologies) vector containing HO-1 digested with BamHI-HF and EcoRI-HF (NEB) with T4 DNA Ligase (Life Technologies).

Native PAGE, SDS-denaturing PAGE, and zinc blot. Native PAGE was run using NativePAGE Novex Bis-Tris Gel System (Life Technologies) on NativePAGE 4–16% Bis-Tris protein gels (Life Technologies). SDS-denaturing PAGE was run using NuPAGE MOPS SDS running buffer (Life Technologies) and NuPAGE Novex 4–12% Bis-Tris gels (Life Technologies). Precision Plus Protein Dual Color Standards (Bio-Rad) were used as an MW ladder. Zinc blot was performed after running the SDS-PAGE gel using the described method⁴⁴. Fluorescence was imaged using a BioSpectrum AC Imaging System (UVP) with EX/EM = 535(45)/605(70) nm for tdTomato, EX/EM = 650(13)/690(50) nm for smURFP and TDsmURFP, EX/EM = 685(40)/710LP nm for IFP1.4 and BV + zinc.

Construction of lentiviral vectors, virus production, and neuron infection. smURFP-T2A-mCherry (GenBank AY678264), smURFP-T2A-mCardinal, smURFP, and mCardinal (Addgene 51311) were subcloned in a generation-two lentiviral vector with the CMV promoter for constitutive expression. Viruses were produced as described⁴⁵. The procedures for extracting cultured neurons from rat pups were approved by the UCSD Institutional Animal Care and Use Committee (IACUC, #S03172R) and are consistent with the recommendations of the American Veterinary Medical Association. Primary cortical neurons were dissociated by papain from postnatal day 2 Sprague Dawley rats ($n = 6$) of either sex and combined, plated on poly-D-lysine-coated glass-bottom culture dishes (MatTek, #P35G-0-14-C), and cultured in Neurobasal A medium + 1× B27 supplement (Life Technologies) + 2 mM GlutaMAX (Life Technologies) + 1× penicillin–streptomycin (Fisher Scientific). Prior to fluorescence imaging, 25 μ M BV was added for 10 min, removed, and washed with 2× 2 ml Hank's Balanced Salt Solution (HBSS, Life Technologies) + 2 g/L glucose + 20 mM HEPES (pH 7.4), referred to as imaging solution. Fluorescence imaging was performed *in vitro* 15 d after infection

using a Zeiss Axiovert 200M inverted microscope controlled by SlideBook software. FPs were imaged as follows: smURFP and TDsmURFP, EX/EM = 628(40)/680(30) nm; and mCherry, EX/EM = 580(20)/653(95) nm.

Fluorescence imaging of HT1080 tumor xenografts *in vivo*. HT1080 cells were infected with CMV with smURFP-T2A-mCherry, smURFP-T2A-mCardinal, smURFP, and mCardinal lentiviruses in culture, and expression was verified by fluorescence imaging (**Supplementary Fig. 14a**, $\geq 99\%$ efficiency and **Supplementary Fig. 15a**, $\geq 95\%$ efficiency) using filters described in the previous section. All procedures using mice were approved by UCSD IACUC (#S03172M) and are consistent with the recommendations of the American Veterinary Medical Association. One million HT1080 cells expressing smURFP-T2A-mCherry were injected subcutaneously into the lateral, ventral, and upper right and left quadrant, or smURFP and mCardinal were injected subcutaneously into the lateral, dorsal, and lower right and left quadrant of four 5-week-old athymic nude female mice. Tumors were allowed to grow until ~0.1–1 cm in diameter (~2 weeks). Mice were anesthetized with isoflurane (1.5%) at a 2 liter/min flow, injected with ketamine–midazolam (intraperitoneal (IP), 80 mg/kg, 4 mg/kg), placed on a heated pad, and imaged before exogenous BV injection. 250 nmol BV was injected by intravenous (IV) tail vein, and mice were imaged 5, 30, 60, and 120 min after BV injection for smURFP-T2A-mCherry. 250 nmol BV or BVMe₂ was injected by intravenous tail vein, and mice were imaged 60 min, 24 h, and 48 h after BV injection for smURFP and mCardinal tumors. Mice were imaged using a Maestro *in vivo* Imaging System (Cambridge Research & Instrumentation, CRI). FPs were imaged with the following filters: mCherry, EX/EM = 590(23)/615LP nm and liquid crystal, 620 nm; mCardinal EX/EM = 607(36)/645LP nm and liquid crystal, 660 nm; and smURFP EX/EM = 620(20)/645LP nm or EX/EM = 640(47)/700LP and liquid crystal, 710 nm. Image cubes were obtained and could be spectrally unmixed, but raw fluorescence images before chromophore injection are shown in **Supplementary Figures 14c and 15f** because no fluorescence increase was seen after 250 nmol BV or BVMe₂ injection. Tumors were removed, washed 2× in 2 ml DMEM + 10% FBS, labeled in 2 ml DMEM + 10% FBS + 10 μ M BV or BVMe₂ at 4 °C for 24 h, imaged, labeled in 2 ml DMEM + 10% FBS + 10 μ M BV or BVMe₂ at 37 °C for 24 h, and imaged (**Supplementary Fig. 15g**).

Plasma collection and BV or BVMe₂ concentration analysis. Whole blood was collected via abdominal aorta and placed in tubes with lithium heparin (BD, No. 365971) on ice. Tubes were centrifuged to remove red blood cells, and plasma was stored on ice for 30 min. Clarified plasma was combined and aliquoted into 9× 70 μ l aliquots and placed on ice. The following nine experiments were performed: starting plasma (1) and plasma + 10 μ M BV (2–5) or BVMe₂ (6–9) at time 0 at 4 °C and 15, 60, and 1,440 min at 37 °C. Reactions were stopped by freezing at –80 °C. Plasma samples were thawed, diluted 4× with cold 50% ACN, 48% water (H₂O), and 2% acetic acid, and centrifuged for 14 min at 4 °C. Reverse-phase high performance liquid chromatography (HPLC) was performed on an Agilent 1100 Series HPLC on a Phenomenex Luna C18(2) reverse-phase column 100 Å, 250 cm × 21.20 mm I.D. 10 μ m reverse-phase column (00G-4253-P0 AX), with a 21 min,

10–90% H₂O:ACN (0.05% trifluoroacetic acid, TFA) gradient and a flow rate of 1 ml/min into a diode array detector and MSD-Ion Trap (Agilent LC/MSD trap XCT). 5 mM BV or BVMe₂ in DMSO was diluted and used to calibrate the concentration of chromophore as a function of peak area (**Supplementary Fig. 16**).

Mammalian expression plasmids, cell culture, transfection, chromophore addition, and fluorescence imaging. smURFP codons were optimized for human cell expression, and the gene was created by GenScript. smURFP, TDsmURFP (created from mammalian-optimized smURFP), IFP1.4 (mammalian-optimized form³⁵), IFP2.0 (mammalian-optimized form⁴⁶), and iRFP713 (mammalian-optimized form³⁶) were PCR amplified using Phusion High-Fidelity DNA Polymerase (NEB) with primers containing 5' HindIII and 3' XhoI restriction enzyme sites. HindIII-HF and XhoI (NEB)-digested PCR fragments were gel purified (Zymoclean Gel DNA Recovery Kit) and were ligated (T4 DNA Ligase, Life Technologies) into a similarly digested pCDNA3-IRES-eGFP vector (bicistronic to express two FPs in the same cell). For creation of HO-1-expressing mammalian vectors, the *Synechocystis* HO-1 was used, and the codons were not optimized for mammalian expression. *Synechocystis* HO-1 was directly amplified from the pBAD vector using primers containing 5' BsiWI and 3' XbaI restriction enzyme sites. pCDNA3 smURFP, TDsmURFP, IFP1.4, IFP2.0, or iRFP713-IRES-eGFP vectors were digested with BsiWI and XbaI (NEB), dephosphorylated (SAP, Roche), gel purified (Zymoclean Gel DNA Recovery Kit), and ligated (T4 DNA Ligase, Life Technologies) with similarly digested, purified HO-1 PCR fragment. For creation of smURFP fusions, smURFP was PCR amplified using Phusion High-Fidelity DNA Polymerase (NEB) with primers containing 5' AgeI and 3' NotI restriction enzyme sites for N-terminal fusions or with primers containing 5' AgeI and 3' BspEI restriction enzyme sites for C-terminal fusions. mGeos2-VEL-ManII-N-10 (Addgene 57551) and Dronpa-PDHA1-N-10 (Addgene 57292) vectors were digested with AgeI and NotI (NEB) and mCherry- α Tubulin-C-18 (Addgene 55148) and tdTomato-LaminB1-10 (Addgene 58107) were digested with AgeI and BspEI, dephosphorylated (SAP, Roche), gel purified (Zymoclean Gel DNA Recovery Kit), and ligated (T4 DNA Ligase, Life Technologies) with similarly digested, purified smURFP PCR fragment. HEK293A (Invitrogen, Life Technologies), HT1080 (ATCC), and PC3 (ATCC) cells were grown in Dulbecco's Modified Eagle's medium (DMEM, Corning), supplemented with 10% FBS (Atlanta Biologicals) + 1 \times penicillin-streptomycin (Fisher Scientific), which is referred to as growth media, on poly-D-lysine-coated glass-bottom culture dishes (MatTek, No. P35G-0-14-C). The HEK cell line is listed in the ICLAC and NCBI biosample databases and is commonly misidentified as the HeLa cell line. For expression of exogenous fluorescent proteins, there is no problem if there is a contaminating cell line because no endogenous biology or therapeutic results are being determined. HEK293A cells were purchased from Invitrogen (Life Technologies), and all experiments are derived from the same expanded frozen stock without cell line authentication or mycoplasma detection. Cells were transfected using 2 μ g of circular DNA + 5 μ l Lipofectamine 2000 (Life Technologies) in 2 ml Opti-MEM (Life Technologies) for 4–5 h, transfection media was discarded, and prewarmed growth media was added. Chromophores (5 mM in DMSO) were added at indicated

concentrations to growth media, warmed for 10–15 min at 37 °C, and added to cells. For multiple timepoints, incubations were staggered to maintain equivalent incubation. Prior to imaging, cells were washed 1 \times 2 ml growth media, 2 \times 2 ml imaging solution, and imaged in 2 ml imaging solution. Fluorescence imaging was performed on a Zeiss Axiovert 200M inverted microscope controlled by SlideBook software. FPs were imaged with the following settings: eGFP, EX/EM = 495(10)/535(25) nm, tdTomato EX/EM = 540(25)/595(50) nm; mCherry and mCardinal, EX/EM = 580(20)/653(95) nm; smURFP and TDsmURFP, EX/EM = 628(40)/680(30) nm; and IFP1.4, IFP2.0, and iRFP713, EX/EM = 665(45)/725(50) nm. When comparing mean fluorescence intensity of FPs with different wavelengths, data was normalized to reflect chromophore absorbance, chromophore extinction coefficient, light power (measured with an IL1700 research radiometer (International Light Technologies)), objective, EX/EM filters transmission, and dichroic reflectance as described³⁷.

FP stability in HEK293A cells. HEK293A cells were transfected with pCDNA3-smURFP-IRES-eGFP and incubated for 48 h. 25 μ M BV or 5 μ M BVMe₂ was added to HEK293A cells as listed in **Supplementary Figure 17**. 50 μ g/ml cycloheximide + 25 μ M BV, 5 μ M BVMe₂, or no chromophore was added and cells were imaged after 1, 10, 30, 60, 120, and 225 min. Fluorescence was fit to a single exponential decay ($F = A[\exp^{-kt}]$), where F is fluorescence that varies as a function of time, A is the fit initial fluorescence, k is the rate of fluorescence decay (protein degradation), and t is time in min. Fitted values and $t_{50\%}$ (calculated by $t_{50\%} = \ln(2)/k$) of FPs are listed in **Supplementary Figure 17**.

Photobleaching FP or FP fusions in mammalian cells. PC3 cells were transfected with 2 μ g of circular DNA + 5 μ l Lipofectamine 2000 (Life Technologies) in 2 ml Opti-MEM (Life Technologies) for 4–5 h, transfection media was discarded, prewarmed growth media was added, and protein was produced for 48 h. 25 μ M BV or 1 μ M BVMe₂ was incubated for 4 h. Cells were photobleached with continuous light exposure from a 150 W xenon arc lamp with eGFP EX/EM = 495(10)/535(25) nm, tdTomato EX/EM = 540(25)/595(50) nm, mCherry EX/EM = 580(20)/53(95) nm, and smURFP EX/EM = 628(40)/680(30) nm focused with a 40 \times , 1.2 numerical aperture C-Apochromat oil-immersion lens on a Zeiss Axiovert 200M inverted microscope. Photobleaching times were normalized to reflect an initial illumination intensity producing 1,000 photons per fluorescent molecule per second as previously described³⁷. Data was fit to a single exponential decay ($F = A[\exp^{-kt}]$), where F is fluorescence that varies as a function of time, A is the fit normalized, initial fluorescence (should be 1), k is the rate of fluorescence decay (photobleaching), and t is time in s, or a double exponential decay ($F = A_1[\exp^{-k_1t}] + A_2[\exp^{-k_2t}]$), where F is fluorescence that varies as a function of time, A_1 and A_2 are the fit normalized, initial fluorescence (sum should be 1), k_1 and k_2 are the rates of fluorescence decay (photobleaching), and t is time in seconds, and data is shown in **Supplementary Table 4**.

Creating and imaging transiently or stably expressing FR and NIR FUCCI in HEK293A cells. pCSII-EF-containing mAG-hGem(1/110) or mKO2-hCdtI(30/120) (A. Miyawaki, RIKEN) were PCR amplified using Phusion High-Fidelity DNA Polymerase

(NEB) with primers containing 5' HindIII-HF and 3' XbaI restriction enzyme sites. HindIII-HF and XbaI (NEB)-digested PCR fragments were gel purified (Zymoclean Gel DNA Recovery Kit) and were ligated (T4 DNA Ligase, Life Technologies) into a similarly digested pCDNA3 vector, creating initial pCDNA3-mAG-hGem(1/110) or mKO2-hCdtI(30/120) vectors. smURFP, TDsmURFP, and IFP2.0 were PCR amplified using Phusion High-Fidelity DNA Polymerase (NEB) with primers containing 5' HindIII and 3' XhoI, HindIII-HF and XhoI digested (NEB), gel purified (Zymoclean Gel DNA Recovery Kit). pCDNA3 mAG-hGem(1/110) or mKO2-hCdtI(30/120) were digested with HindIII-HF and XhoI (NEB) to remove the FP and linker, dephosphorylated (SAP, Roche), and gel purified (Zymoclean Gel DNA Recovery Kit). pCDNA3 X-hGem(1/110) or hCdtI(30/120) were ligated with smURFP, TDsmURFP, and IFP2.0 to create pCDNA3 smURFP, TDsmURFP, or IFP2.0-hGem(1/110) or hCdtI(30/120), six plasmids with hygromycin B resistance to create stable cell lines.

HEK293A cells were transfected with Lipofectamine 2000 (Life Technologies) on glass-bottom dishes (grown and transfected as described above). Initially, all eight constructs (including mAG-hGem(1/110) and mKO2-hCdtI(30/120)) were fluorescently imaged using a Zeiss Axiovert 200M inverted microscope controlled by SlideBook software. FPs were imaged as follows: mAG EX/EM = 495(10)/535(25) nm, mKO2 EX/EM = 540(25)/595(50) nm, smURFP or TDsmURFP EX/EM = 628(40)/680(30) nm, and IFP2.0 EX/EM = 665(45)/725(50) nm. smURFP, TDsmURFP, or IFP2.0-hGem(1/110) or hCdtI(30/120) all had fluorescent nuclei when transiently expressed in HEK293A cells. A kill curve was generated with hygromycin B (Life Technologies) and 300 µg/ml hygromycin B was sufficient to kill untransfected HEK293A cells. HEK293A cells expressing mAG or IFP2.0-hGem(1/110) or mKO2 or IFP2.0-hCdtI(30/120) were grown for 3 weeks in growth media + 300 µg/ml hygromycin B. Cells were selected using fluorescently activated cell sorting (FACS) using FACSDiVa (BD Biosciences) to give an enriched stable population containing the expressed FP fusion. Cells expressing FPs were sorted using the following filters: mAG EX/EM = 488/535(20) nm, mKO2 EX/EM = 568/610(40) nm, and IFP2.0 EX/EM = 670/710LP nm. HEK293A cells expressing mAG or IFP2.0-hGem(1/110) were transfected with smURFP or TDsmURFP-hCdtI(30/120), or mKO2 or IFP2.0-hCdtI(30/120) were transfected with smURFP or TDsmURFP-hGem(1/110) and grown for an additional 3 weeks in growth media + 300 µg/ml hygromycin B. 198 individual clones were FACS (smURFP EX/EM = 647(10)/675(20) nm) for the eight combinations and grown for 2 weeks. Clones were initially assayed to verify both FPs and then proper growth (many cells show no growth and/or decreased cell cycle progression, which was typically accompanied by higher FP-fusion expression). TDsmURFP fusions were dimmer than smURFP fusions and were not characterized further. IFP2.0-hCdtI(30/120) or smURFP-hGem(1/110) fluorescence was lacking and/or extremely dim and could not be visualized with smURFP-hGem(1/110) or mKO2-hCdtI(30/120), respectively. mAG-hGem(1/110) + smURFP-hCdtI(30/120) and IFP2.0-hGem(1/110) + smURFP-hCdtI(30/120) (FR and NIR FUCCI) had sufficient fluorescence, and three clones of each were grown and reanalyzed for fluorescence of both FPs and adequate growth. A single clone of each was imaged by time-lapse fluorescence microscopy.

Time-lapse imaging of FUCCI HEK293A cells. HEK293A cells stably expressing FUCCI were grown in growth media on glass-bottom dishes coated with poly-D-lysine. After 2 d, media was changed to 2 ml Leibovitz L-15 medium (no phenol red, Life Technologies) + 1 g/L glucose + 200 µM Trolox + 200 µM L-ascorbic acid + 12.5 µM BV for 1 d. A Zeiss Axiovert 200M inverted microscope with temperature control chamber was allowed to equilibrate at 37 °C for ~30 min and HEK293A FUCCI cell-imaging dish was placed on the stage. The plastic lid was removed and 2.2 ml of mineral oil was added to the top (ensuring complete seal to avoid media evaporation). A metal imaging dish weight sealed with a glass coverslip was placed on top of the imaging chamber to avoid focus drift during imaging. The microscope + dish were equilibrated for ~1 h at 37 °C. Cells were imaged every 15 min using a 10% neutral density filter. FPs were imaged as follows: mAG-hGem(1/110) EX/EM = 488/535(20) nm, smURFP-hCdtI(30/120) EX/EM = 628(40)/680(30) nm, and IFP2.0-hGem(1/110) EX/EM = 665(45)/725(50) nm. Movies were created in ImageJ⁴⁷. All three image channels (DIC, smURFP-hCdtI(30/120), and mAG or IFP2.0-hGem(1/110)) were opened separately as a hyperstack and brightness and contrast were adjusted as desired. The time was added to the DIC stack using Time Stamper (ImageJ plugin) and the three channels were merged using the following pseudocoloring: red, smURFP-hCdtI(30/120); green, mAG or IFP2.0-hGem(1/110); and gray, DIC. The AVI movie was exported using JPEG compression and ten frames per second in ImageJ. AVI movies were converted to MOV movies using QuickTime Player (Version 10.4, Apple).

Experimental setup, data analysis, and statistical methods.

For cell culture experiments, sample sizes of $\geq n = 30$ cells (n listed with each experiment) were chosen to ensure P values < 0.03 for the majority of significant comparisons. For animal experiments, four mice with two tumors each ($n = 8$ tumors) were chosen arbitrarily to ensure reproducibility of results. No cell culture dishes or animals were excluded from analysis for any reason. For animal studies, no randomization or blinding was used because both mCherry and smURFP FPs were simultaneously expressed on a bicistronic mRNA in each tumor cell that made up the tumor, or smURFP and mCardinal tumors were imaged simultaneously on the same mouse. Tumors were imaged with both sets of excitation and emission filters. Fluorescence images were adjusted and analyzed using ImageJ⁴⁷. Graphs, statistics, and statistical significance tests were generated using KaleidaGraph 4.1 (Synergy). Comparisons were performed on mean fluorescence intensity with a one-way ANOVA with significance level set at $\alpha = 0.05$. Equivalence of variance was determined for the one-way ANOVA with a *post hoc* test of Tukey honestly significant difference (HSD) for comparisons between any two samples. All error bars are s.e.m., except **Figure 3a,b** is calculated as error propagation of the s.e.m.

DNA constructs. GenBank/EMBL/DDBJ: smURFP, KX449134; TDsmURFP, KX449135. Bacterial and mammalian expression plasmids and lentiviral transfer vectors are available at Addgene: smURFP, 80341, 80343, 80345, 80347, 80348, 80349; and TDsmURFP, 80342, 80344, 80346.

33. Toettcher, J.E., Gong, D., Lim, W.A. & Weiner, O.D. Light control of plasma membrane recruitment using the Phy-PIF system. *Methods Enzymol.* **497**, 409–423 (2011).
34. Gambetta, G.A. & Lagarias, J.C. Genetic engineering of phytochrome biosynthesis in bacteria. *Proc. Natl. Acad. Sci. USA* **98**, 10566–10571 (2001).
35. Shu, X. *et al.* Mammalian expression of infrared fluorescent proteins engineered from a bacterial phytochrome. *Science* **324**, 804–807 (2009).
36. Filonov, G.S. *et al.* Bright and stable near-infrared fluorescent protein for *in vivo* imaging. *Nat. Biotechnol.* **29**, 757–761 (2011).
37. Shaner, N.C., Steinbach, P.A. & Tsien, R.Y. A guide to choosing fluorescent proteins. *Nat. Methods* **2**, 905–909 (2005).
38. Arnold, K., Bordoli, L., Kopp, J. & Schwede, T. The SWISS-MODEL workspace: a web-based environment for protein structure homology modelling. *Bioinformatics* **22**, 195–201 (2006).
39. Liu, J.Y., Jiang, T., Zhang, J.P. & Liang, D.C. Crystal structure of allophycocyanin from red algae *Porphyra yezoensis* at 2.2-Å resolution. *J. Biol. Chem.* **274**, 16945–16952 (1999).
40. Schneidman-Duhovny, D., Inbar, Y., Nussinov, R. & Wolfson, H.J. PatchDock and SymmDock: servers for rigid and symmetric docking. *Nucleic Acids Res.* **33**, W363–W367 (2005).
41. Andrusier, N., Nussinov, R. & Wolfson, H.J. FireDock: fast interaction refinement in molecular docking. *Proteins* **69**, 139–159 (2007).
42. Larkin, M.A. *et al.* Clustal W and Clustal X version 2.0. *Bioinformatics* **23**, 2947–2948 (2007).
43. Pettersen, E.F. *et al.* UCSF Chimera—a visualization system for exploratory research and analysis. *J. Comput. Chem.* **25**, 1605–1612 (2004).
44. Wahleithner, J.A., Li, L.M. & Lagarias, J.C. Expression and assembly of spectrally active recombinant holophytochrome. *Proc. Natl. Acad. Sci. USA* **88**, 10387–10391 (1991).
45. Lin, J.Y., Knutsen, P.M., Muller, A., Kleinfeld, D. & Tsien, R.Y. ReaChR: a red-shifted variant of channelrhodopsin enables deep transcranial optogenetic excitation. *Nat. Neurosci.* **16**, 1499–1508 (2013).
46. Yu, D. *et al.* An improved monomeric infrared fluorescent protein for neuronal and tumour brain imaging. *Nat. Commun.* **5**, 3626 (2014).
47. Schneider, C.A., Rasband, W.S. & Eliceiri, K.W. NIH Image to ImageJ: 25 years of image analysis. *Nat. Methods* **9**, 671–675 (2012).

Corrigendum: A far-red fluorescent protein evolved from a cyanobacterial phycobiliprotein

Erik A Rodriguez, Geraldine N Tran, Larry A Gross, Jessica L Crisp, Xiaokun Shu, John Y Lin & Roger Y Tsien
Nat. Methods. 13, 763–769 (2016); published online 1 August 2016; corrected after print 16 September 2016

In the version of this article initially published, Roger Y. Tsien was listed as the corresponding author. On account of his sad demise shortly after publication, Erik A. Rodriguez has been added as corresponding author. This has been updated in the HTML and PDF versions of the article.